A preliminary assessment of the electron cloud effect for the FNAL main injector upgrade*

M. A. Furman†
Center for Beam Physics
Lawrence Berkeley National Laboratory, Bldg. 71R0259
1 Cyclotron Rd.
Berkeley, CA 94720
(Dated: 23 June 2006)

We present results from a preliminary assessment, via computer simulations, of the electron-cloud density for the FNAL main injector (MI) upgrade at injection energy. Assuming a peak value for secondary emission yield $\delta_{\max} = 1.3$, we find a threshold value of the bunch population, $N_{b,th} \simeq 1.25 \times 10^{11}$, beyond which the electron-cloud density ρ_e reaches a steady-state level that is $\sim 10^4$ times larger than for $N_b < N_{b,th}$, essentially neutralizing the beam, and leading to a tune shift ~ 0.05. Our investigation is limited to a field-free region and to a dipole magnet region, both of which yield similar results for both $N_{b,th}$ and the steady-state value of ρ_e. Possible dynamical effects from the electron cloud (EC) on the beam, such as emittance growth and instabilities, remain to be investigated separately.

I. INTRODUCTION AND SUMMARY.

An upgrade to the MI at FNAL is being considered [1] which would increase the bunch intensity N_b by a factor of 5 from its present value of 6×10^{10}. Such an increase would place the MI in a regime in which a significant electron-cloud effect has been observed at other hadron machines [2–5].

In this article we present an examination of the EC at the MI by means of computer simulations with the code POSINST [6–9]. For the purposes of the present work, we fix two important parameters, namely the beam energy E at its injection value, and the peak value $\delta_{\max}$ of the secondary emission yield (SEY) of the vacuum chamber at 1.3. Furthermore, we confine our attention to only two regions of the ring: a drift, and a dipole magnet of strength $B = 0.1$ T. More specifically, we compute the electron density ρ_e as a function of N_b, and we consider two models of the SEY that differ in the emitted-energy spectrum at fixed $\delta_{\max}$. We find a threshold value for the bunch intensity, $N_{b,th} \simeq 1.25 \times 10^{11}$, beyond which ρ_e grows exponentially in time with an e-folding time $\tau \simeq 100$ ns upon injection into an empty ring, and reaches a steady-state value that is 10^4 times larger than for $N_b < N_{b,th}$. In steady state, for $N_b > N_{b,th}$, the EC essentially neutralizes the beam and leads to a tune shift $\Delta\nu \sim 0.05$. An assessment of possible dynamical effects on the beam from the EC, such as emittance growth and instabilities, falls outside the scope of this article, as does a systematic sensitivity analysis of our results on various assumed input parameters, particularly $\delta_{\max}$.

*Work supported by the US DOE under contract DE-AC03-76SF00098.
†Electronic address: mafurman@lbl.gov; URL: http://mafurman.lbl.gov

II. ELECTRON SOURCES.

A. Primary mechanisms.

In general, the build-up of the electron cloud (EC) is seeded by primary electrons from three main sources: photoelectrons, ionization of residual gas, and electrons produced by stray beam particles striking the chamber wall. Since these processes are essentially incoherent, it is customary to quantify them in terms of the number of primary electrons produced per beam particle per unit length of beam traversal, n'_e. For the MI, the contribution to the primary electron density from photoelectrons is wholly negligible. The contribution from residual gas ionization can be estimated from the gas density. The inverse of the mean free path for an ionization event by a particle traveling in a gas is given by $\rho_g \sigma_i$, where σ_i is the ionization cross-section and ρ_g the gas density. Expressing ρ_g in terms of the pressure P and temperature T yields

$$n'_{e(i)}\,[\mathrm{m}^{-1}] = 3.3\,\sigma_i\,[\mathrm{Mbarn}] \times P\,[\mathrm{Torr}] \times \frac{294}{T\,[\mathrm{K}]}. \quad (1)$$

Implicit in this formula is the assumption that the ionization event yields a single electron. A typical value for σ_i, which we assume in this note, is 2 Mbarns [10] (for simplicity, we neglect here the dependence of σ_i on beam energy). Assuming $P = 20$ nT and $T = 305$ K, Eq. (1) yields $n'_{e(i)} = 1.27 \times 10^{-7}$ (e/p)/m.

The contribution from stray protons striking the chamber walls is given by

$$n'_{e(pl)} = \eta_{\mathrm{eff}}\, n'_{pl} \quad (2)$$

where n'_{pl} is the number of lost protons per stored proton per unit length of beam traversal, and η_{eff} is the effective electron yield per proton-wall collision ("*pl*" stands for "proton loss"). We focus on the beam injection process,

since the most significant fraction of beam loss ($f = 1.2\%$ of the beam) occurs during this time, which lasts for $\Delta t_{\rm inj} = 0.4$ s or $N_{\rm inj} = 3.59 \times 10^4$ turns. Assuming that the beam losses occur uniformly throughout the machine circumference C, and uniformly during $\Delta t_{\rm inj}$, we obtain

$$n'_{pl} = \frac{f}{CN_{\rm inj}} = 10^{-10} \quad \text{p/m}. \tag{3}$$

The effective electron yield per proton-wall collision $\eta_{\rm eff}$ has been estimated [11] at the PSR to be $\eta_{\rm eff} \simeq 100-200$. Although $\eta_{\rm eff}$ is a function of the beam energy ($E = 1.7$ GeV for the PSR vs. 8.9 GeV for the case considered here), we set $\eta_{\rm eff} = 100$ for definiteness, hence Eq. (2) yields $n'_{e(pl)} = 10^{-8}$ (e/p)/m. The total primary-electron production rate, therefore, is

$$n'_e = n'_{e(pl)} + n'_{e(i)} = 1.37 \times 10^{-7} \quad \text{(e/p)/m} \tag{4}$$

and the number of primary electrons generated by one bunch passage through a section of length L is given by

$$N_e = n'_e L N_b = 4116 \tag{5}$$

where the numerical value corresponds to the choices $L = 0.1$ m and $N_b = 3 \times 10^{11}$.

As for the time dependence of n'_e, the fact that the primary electron-generation processes are incoherent implies that $n'_e(t) \propto I_b(t)$ where $I_b(t)$ is the instantaneous beam current at the ring location under investigation [12].

As mentioned above, and as illustrated below, the primary electrons act primarily as seeds in the formation of the EC when the beam current is above threshold. In this regime, secondary electron emission typically contributes several orders of magnitude more electrons to the EC density, hence the precise values of the primary electron parameters have little impact on the EC in steady state. For this reason we have not attempted to accurately pin them down.

B. Secondary electron emission.

The secondary emission yield (SEY) function $\delta(E_0, \theta_0)$ is the average number of electrons emitted when an electron of kinetic energy E_0 impinges on a surface at an incident angle θ_0 (conventionally measured relative to the normal to the surface). The SEY reaches a peak value $\delta_{\rm max}$ (conventionally specified at normal incidence) at an energy $E_0 = E_{\rm max}$. A fairly detailed phenomenological probabilistic description of the secondary emission process is presented in Refs. 8, 9, upon which we base the analysis in this article.

Closely related to δ is the emitted-energy spectrum of the secondary electrons, $d\delta/dE$ at given incident energy E_0, where E is the emitted electron energy. The spectrum covers the region $0 \le E \lesssim E_0$, and it exhibits three fairly distinct main components: elastically reflected electrons (δ_e), rediffused (δ_r), and true secondaries (δ_{ts}). The SEY is given by $\delta = \delta_e + \delta_r + \delta_{ts}$. The three components are emitted with qualitatively different energy spectra. Depending upon various features of the storage ring considered, the three components can contribute differently to various aspects of the ECE.

Since we do not have data for the SEY of the MI vacuum chamber, for the discussions in this note we adopt two models, which we call "K" and "H," that may be considered representative of the possible range of SEY parameters for the MI. These models correspond, respectively, to the fits to stainless steel and copper data in Refs. 8 and 9, except that in the present article we scale all three components of δ by a common factor so that $\delta_{\rm max} = 1.3$ instead of the original value 2.05. This scaling has the consequence that $\delta(0)$ becomes proportional to $\delta_{\rm max}$. Since we do not know the precise value of $\delta(0)$, this scaling is intended only as a practical step in the parameter exploration, and is not meant to reflect the phenomenology of the secondary emission process.

As seen in Fig. 1, the SEY functions $\delta(E_0)$ are essentially the same for the two models, but the emitted energy spectra are not: the SEY for model K has a larger backscattered component (composed of elastic plus rediffused electrons) than model H (see Table I). When these two models are applied to the estimate of the EC power deposition in the LHC arc dipoles, for example, one finds significantly different results [12], underscoring the importance of the emission spectrum.

The choice $\delta_{\rm max} = 1.3$ used here is meant as a first step of a more complete assessment that is yet to be carried out. It is likely that $N_{b,th}$ is sensitive to $\delta_{\rm max}$ and to other variables. In practice, the value of $\delta_{\rm max}$ is a function of the conditioning state of the material, as it decreases monotonically with electron bombardment. Vacuum chambers made of copper or stainless steel have $\delta_{\rm max}$ values in the range $\sim 1.5 - 2.5$, or even higher, in the "as-received" condition. For aluminum, the values are typically higher than this. Bench experiments show that, if the material is bombarded in vacuum with a steady flow of electrons, $\delta_{\rm max}$ decreases to ~ 1.1 after a dose ~ 1 C/cm^2 [13–16]. The MI vacuum chamber is made of stainless steel; our choice $\delta_{\rm max} = 1.3$ is generally believed to correspond to a more or less well-conditioned state of this material. However, the sensitivity of our results to $\delta_{\rm max}$ is an important issue that remains to be investigated.

III. ELECTRON-CLOUD BUILD-UP.

A. General considerations.

A convenient phenomenological parameter to characterize the EC build-up (and decay) is the effective SEY, $\delta_{\rm eff}$, defined as an average over a time window of the convolution of $\delta(E_0, \theta_0)$ with the energy-angle electron-wall

TABLE I: Assumed MI parameters for EC simulations at injection.

Parameter	Symbol (unit)	Value
Ring and beam parameters		
Ring circumference	C (m)	3319.419
Beam energy	E_b (GeV)	8[a]
Relativistic beam factor	γ_b	8.526312
Revolution period	T_0 (μs)	11.1493
Beam pipe cross section	$\cdots$	elliptical
Beam pipe semi-axes	(a, b) (cm)	(6.15,2.45)
Harmonic number	h	588
RF wavelength	$\lambda_{\rm RF}$ (m)	5.645270
No. bunches per beam	$\cdots$	504
Bunch spacing	s_b (m)	5.645270
Gap length	$\cdots$ (buckets)	84
Bunch population	N_b	$(0.6-3)\times10^{11}$
RMS bunch length	σ_z (m)	0.75
Longit. bunch profile	$\cdots$	gaussian
Transverse bunch profile	$\cdots$	gaussian
Average beta function	$\bar{\beta}$ (m)	25
Normalized tr. emittance (95%)	ϵ_N (m-rad)	40π
RMS relative momentum spread	σ_p/p	10^{-3}
Transverse RMS bunch sizes	(σ_x, σ_y) (mm)	(5,5)
Parameters for primary e^- sources		
Proton loss rate	n'_{pl} (p/m)	1×10^{-10}
Proton-electron yield	$\eta_{\rm eff}$	100
Residual gas pressure	P (nTorr)	20
Temperature	T (K)	305
Ionization cross-section	σ_i (Mbarns)	2
Proton-loss e^- creation rate	$n'_{e(pl)}$ ((e/p)/m)	1×10^{-8}
Ionization e^- creation rate	$n'_{e(i)}$ ((e/p)/m)	1.27×10^{-7}
Secondary e^- parameters		
Peak SEY	$\delta_{\rm max}\equiv\delta(E_{\rm max})$	1.3[b,c]
Energy at peak SEY	$E_{\rm max}$ (eV)	293[b], 272[c]
SEY at 0 energy	$\delta(0)$	0.32[b], 0.38[c]
Backscattered component at $E_{\rm max}$	$\delta_e(E_{\rm max})+\delta_r(E_{\rm max})$	0.53[b], 0.13[c]
Simulation parameters		
Simulated section	$\cdots$	drift or dipole magnet
Length of simulated region	L (m)	0.1
Dipole magnet field	B (T)	0.1
No. kicks/bunch	N_k	11
(Full bunch length)/(RMS bunch length)	L_b/σ_z	4
No. steps between bunches	N_g	9
No. primary macroelectrons/bunch	M_e	10
Macroelectron charge at $N_b=3\times10^{11}$	Q/e	412
Time step size	Δt (ns)	1

[a] See footnote 2.

[b] Model "K".

[c] Model "H".

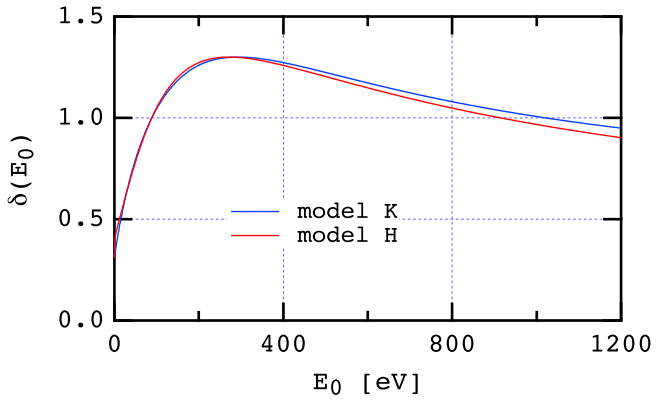

FIG. 1: The SEY at normal incidence ($\theta_0 = 0$) for both models used as input to the simulations.

collision spectrum (normalized to unity) $dN/dE_0 d\theta_0$,

$$\delta_{\rm eff} = \int dE_0 d\theta_0 \, \frac{dN}{dE_0 d\theta_0} \delta(E_0, \theta_0). \tag{6}$$

The spectrum $dN/dE_0 d\theta_0$ is a function of many variables such as the bunch intensity and fill pattern, the vacuum chamber geometry, etc. This spectrum is not known a priori, and hence neither is $\delta_{\rm eff}$. Nevertheless, in general, $\delta_{\rm eff}$ has a monotonic dependence on $\delta_{\rm max}$. In effect, the integral in Eq. (6) is evaluated during the simulation process: $\delta_{\rm eff}$ is obtained by dividing the number of emitted electrons by the number of incident electrons during any given time window.

When $\delta_{\rm eff} < 1$ the chamber walls act as net absorbers of electrons, and the EC build-up is dominated by the production of primary electrons. Since the beam, on average, produces a fixed number of primary electrons per unit time, the EC line density at a given location in the ring, $\lambda_e(t)$, grows linearly in time t following injection of the beam into an empty chamber according to

$$\lambda_e(t) \simeq \bar{\lambda}_b \dot{n}_e t \tag{7}$$

where $\bar{\lambda}_b = eN_b/s_b$ is the average beam line density and $\dot{n}_e$ is the number of primary electrons generated per beam particle per unit time, $\dot{n}_e = n'_e v_b$, where v_b is the beam velocity. After a growth time τ, the EC line density reaches saturation when the number of primary electrons generated per unit time equals the number of electrons absorbed by the walls per unit time. The saturated value of the time constant τ and λ_e are given by [17]

$$\tau = \frac{\Delta_{tr}}{1 - \delta_{\rm eff}} \qquad (\delta_{\rm eff} < 1) \tag{8a}$$

$$\bar{\lambda}_e = \bar{\lambda}_b \dot{n}_e \tau \tag{8b}$$

where Δ_{tr} is the characteristic traversal time of the electrons across the chamber under the action of the beam. This situation typically happens when N_b and/or $\delta_{\rm max}$ are low, although it can also happen when N_b is very large owing to the fall-off of $\delta(E_0)$ at very high E_0. If the production of primary electrons ceases (for example, when the beam is extracted, or during a gap in the bunch train), the EC density decays exponentially in time if the space-charge forces are negligible [12].[1]

If, on the other hand, $\delta_{\rm eff} > 1$, the EC build-up is dominated by secondary electron emission quickly following injection of the beam into an empty chamber on account of the inherently compound effect of secondary emission: the more electrons are present, the more are generated. In this case the average EC density grows exponentially in time until a saturation is reached when the space-charge forces from the EC suppress further secondary emission from the walls. The saturation level reached by the EC density is insensitive to n'_e. It does not grow indefinitely as $\delta_{\rm eff} \to 1^-$, as Eqs. (8a-8b) might imply, but rather reaches a limit comparable to the beam neutralization level. This situation happens when N_b and/or $\delta_{\rm max}$ are sufficiently high. In the exponential growth regime, the growth time τ of the EC density is related to $\delta_{\rm eff}$ and Δ_{tr} by [12]

$$\delta_{\rm eff} = e^{\Delta_{tr}/\tau} \qquad (\delta_{\rm eff} > 1). \tag{9}$$

The traversal time Δ_{tr} is also an "effective" quantity in the same sense that $\delta_{\rm eff}$ is, namely it is an average of the traversal time of all electrons crossing the chamber over their energy and angles. Δ_{tr} is a function of the beam intensity and fill pattern, external magnetic fields, etc. As discussed below, both situations ($\delta_{\rm eff} < 1$ and $\delta_{\rm eff} > 1$) can be realized in the MI, depending upon the value of N_b.

B. Results for the Main Injector.

For the studies presented in this note we have used the simulation code POSINST [6–9]. We consider only two regions of the MI: a drift, and a dipole magnet of field $B = 0.1$ T, and we fix the beam energy at its injection value, $E_b = 8$ GeV.[2] Since the longitudinal motion of the electrons is negligible over the time scales of interest, we perform separate simulations for these two sections. The simulation is restricted to the dynamics of the EC under the action of successive passages of bunches during one machine revolution. The beam is represented by a prescribed function of space and time, hence it is not dynamical. Therefore, aside from the tune shift estimate discussed below, all dynamical effects from the EC on the

[1] The simpler arguments used in Ref. 12 lead to $\tau = -\Delta_{tr}/\ln\delta_{\rm eff}$, which agrees with Eq. (8a) only when $\delta_{\rm eff} \simeq 1$. A fuller discussion will be presented in Ref. 17.

[2] Owing to a misunderstanding, we erroneously chose 8 GeV in our simulations instead of the actual value of 8.9 GeV. The slightly lower value has a negligible effect on our simulation results, except possibly that it leads to an overestimate of the tune shift, Eq. (10), by $\sim 10\%$.

beam, including single-bunch and multi-bunch instabilities, emittance growth, etc., remain to be addressed.

Simulation parameters for the MI used here are listed in Table I. For the above-stated reasons, the length of the simulated region has negligible impact on our results, so we fix it at 0.1 m for definiteness. For the purposes of a first exploration of parameter space, we choose the bunch population N_b in the range $6\times10^{10} \le N_b \le 3\times10^{11}$ while we fix $\delta_{\max} = 1.3$. We carry out simulations for one revolution period ($T_0 = 11.15$ μs) for a MI beam consisting of 504 full buckets followed by a gap of 84 buckets. A brief discussion on the SEY model dependence is presented in Sec. IV.

Figure 2 shows the time evolution of the EC line density. The above-mentioned behaviors are clearly seen. For $N_b = 6\times10^{10}$, the EC reaches an average line density $\bar\lambda_e \simeq 1\times10^{-5}$ nC/m for a drift and $\bar\lambda_e \simeq 2\times10^{-5}$ nC/m for a dipole, while for $N_b = 3\times10^{11}$, the EC density saturates at $\bar\lambda_e \simeq 5.5$ nC/m for both cases. This latter value should compared with the average beam line density, $\bar\lambda_b = 8.5$ nC/m, implying an average beam neutralization factor $\bar\lambda_e/\bar\lambda_b \simeq 0.65$. The exponential growth of the EC density for $N_b = 3\times10^{11}$ is clearly seen over 4 orders of magnitude in density during the first $\sim$1.5 μs, with a growth time $\tau \simeq 110$ ns for the drift and $\tau \simeq 90$ ns for the dipole.

Figure 3 shows the time- and space-averaged electron-wall collision energy spectrum. For $N_b = 6\times10^{10}$, the spectra are sharply cut off at $E_0 \lesssim 200$ eV and yield an average electron-wall collision energy $\sim 50-100$ eV, while for $N_b = 3\times10^{11}$ the spectra exhibit a high-energy tail up to ~ 500 eV, with an average $\sim 100-150$ eV. Referring to Fig. 1, these averages explain qualitatively why $\delta_{\rm eff} < 1$ in the first case while $\delta_{\rm eff} > 1$ in the second.

To assess the simple model embodied by equations (7–9), we consider the results for a drift, specifically the EC build-up in Fig. 2a. For $N_b = 6\times10^{10}$ the values for $\delta_{\rm eff}$, τ and Δ_{tr} obtained directly from the simulation are ~ 0.85, ~ 140 ns and ~ 21 ns, respectively, which satisfy Eq. (8a) well. Furthermore, using $\bar\lambda_e \simeq 1\times10^{-5}$ nC/m from the figure, we obtain from (8b) $\tau = \bar\lambda_e/(\bar\lambda_b\dot n_e) \simeq 140$ ns, in good agreement with the direct result from the simulation. The above value of Δ_{tr}, in turn, implies a typical electron energy ~ 45 eV, in agreement with the direct results from the simulation shown in Fig. 3a. For $N_b = 3\times10^{11}$ we obtain $\delta_{\rm eff} \simeq 1.15$ and $\tau \simeq 110$ ns during the exponential growth regime. Eq. (9) implies $\Delta_{tr} = 15$ ns, which implies an electron energy ~ 90 eV. This value is lower by a factor ~ 2 than what is independently deduced from the simulation (eg., Fig. 3b), presumably owing to the excessive simplicity of the model. The results for a dipole are in qualitative agreement with the above results for a drift.

A straightforward consequence of the EC density is a tune shift $\Delta\nu$ owing to the focusing effect of the electrons on the beam. Assuming that the EC density distribution is round in the transverse plane, the tune shift per unit length of beam traversal through the cloud, $\Delta\nu/L$, is

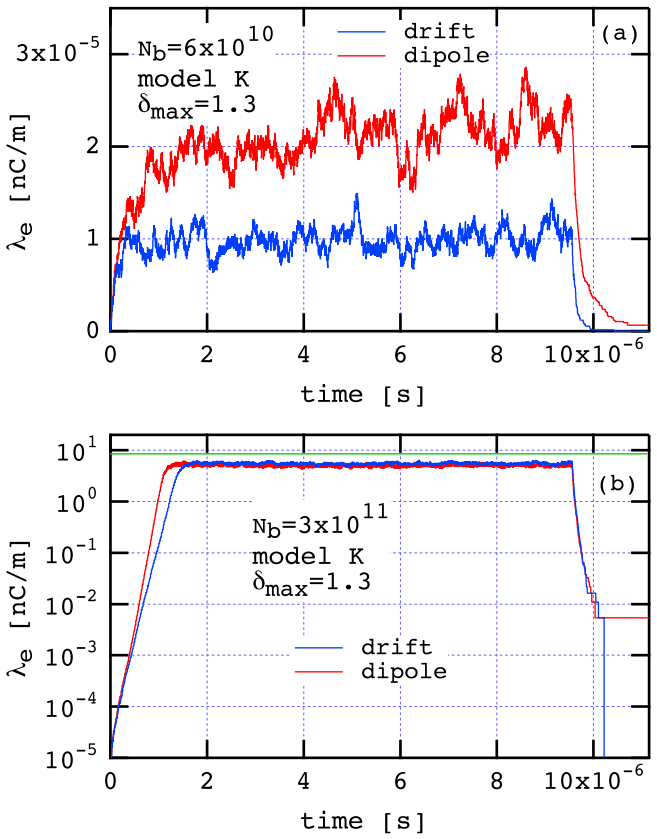

FIG. 2: Average EC line density vs. time. (a): $N_b = 6\times10^{10}$; (b): $N_b = 3\times10^{11}$. Note that the vertical scale for (a) is linear while that for (b) is logarithmic. The exponential growth of the density for case (b) during the first $\sim$1.5 μs has an e-folding time $\tau \simeq 110$ ns for a drift and $\tau \simeq 90$ ns for a dipole. The saturation level is $\bar\lambda_e \simeq 5.5$ nC/m for both cases. For case (b) the horizontal green line represents the average beam line density, $\bar\lambda_b = eN_b/s_b = 8.5$ nC/m.

given by [18]

$$\Delta\nu/L = \frac{r_p\beta\rho_e}{2\gamma_b} \tag{10}$$

where $r_p = 1.535\times10^{-18}$ m is the classical proton radius, γ_b is the relativistic factor of the beam, ρ_e is the EC density (with dimensions of volume^{-1}) seen by the center of the bunch, and β is the usual lattice beta function. For $N_b = 3\times10^{11}$ the steady-state value of the density is $\rho_e \simeq 7.5\times10^{12}$ m^{-3}. Assuming a value of 25 m for the average beta function, we obtain

$$\Delta\nu/L \simeq 1.7\times10^{-5} \quad \text{m}^{-1}. \tag{11}$$

To get an idea of the magnitude of $\Delta\nu$, we replace L by the circumference C, yielding $\Delta\nu = 0.056$. For $N_b < N_{b,th}$, the electron density is $\sim 10^8$ m^{-3}, hence $\Delta\nu \sim 5\times10^{-6}$.

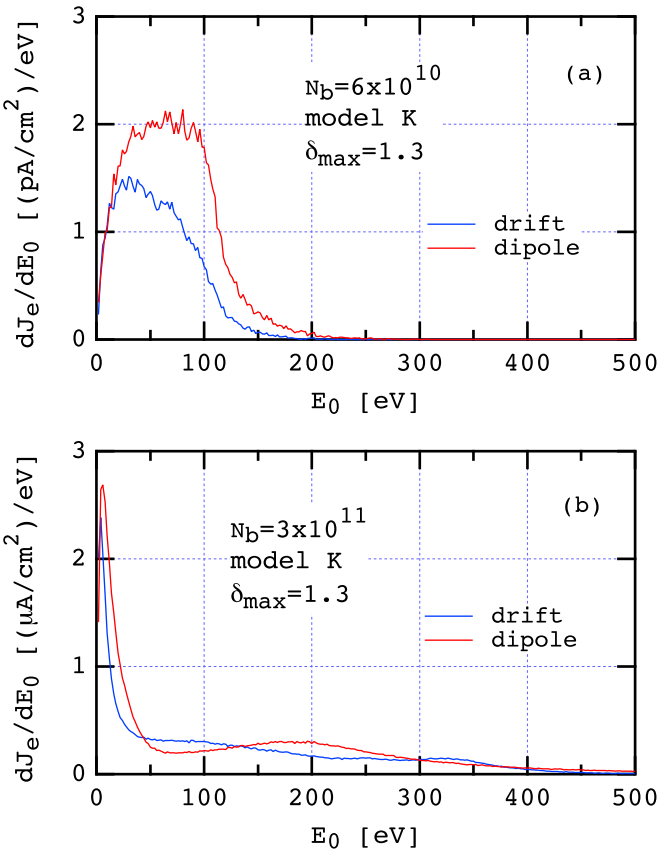

FIG. 3: Energy spectrum of the electrons striking the chamber. (a): $N_b = 6 \times 10^{10}$; (b): $N_b = 3 \times 10^{11}$. Note that there is a factor of 10^6 difference in the vertical scale between cases (a) and (b). The spectrum is averaged over time during one revolution and over the entire surface of the chamber section being simulated, and integrated over incident angles θ_0. The spectrum is normalized so that its integral over E_0 yields the incident-electron flux at the wall, J_e. For case (a), $J_e \simeq 130$ pA/cm^2 for a drift, and $J_e \simeq 220$ pA/cm^2 for a dipole magnet, while for case (b), the corresponding values are $J_e \simeq 100$ μA/cm^2 and $J_e = 130$ μA/cm^2, respectively.

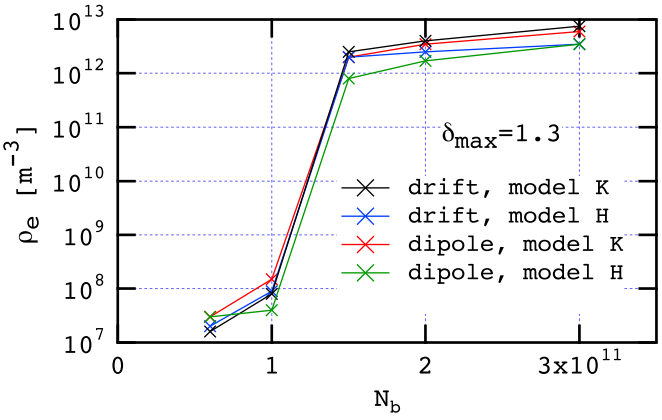

FIG. 4: Steady-state EC density near the bunch center vs. bunch intensity N_b. A threshold in the interval $1.0 \times 10^{11} < N_{b,th} < 1.5 \times 10^{11}$ is evident.

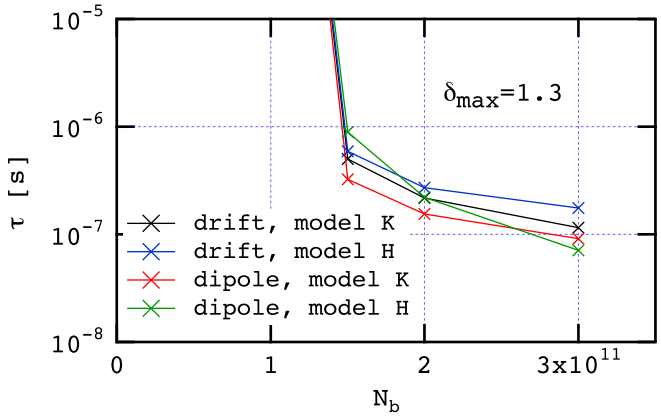

FIG. 5: EC growth time τ vs. bunch intensity N_b. Since τ is expected to $\to \infty$ when $N_b \to N^+_{b,th}$, we have arbitrarily set $\tau = 1$ s for $N_b \leq 1 \times 10^{11}$ for the purposes of this plot.

IV. DISCUSSION.

Figure 4 summarizes the results for the electron density at saturation as a function of N_b. A threshold value for N_b, $N_{b,th} \simeq 1.25 \times 10^{11}$, is strongly indicated both for drifts and dipoles, which seems fairly insensitive to the SEY model. The saturated value of ρ_e, on the other hand, shows a sensitivity to the SEY model on the level of a factor of $\sim$2. Figure 5 shows the growth time τ of the EC density upon injection into an empty chamber, and Fig. 6 the effective SEY $\delta_{\rm eff}$. As is the case for ρ_e, τ and $\delta_{\rm eff}$ show some sensitivity to the model, but $N_{b,th}$ does not (the non-smooth behavior in the dipole cases in Figs. 4-6 for low N_b is probably due to the fact that the EC has not quite reached steady state after one turn, as is apparent in Fig. 2a for $N_b = 6 \times 10^{10}$).

Although the assessment presented in this article is limited, this threshold dependence is the most striking conclusion. Above threshold, the EC density is high enough to lead to a tune shift ~ 0.05. However, owing to the intrinsic limitations of the simulation technique used, we cannot assess the dynamical effects upon the beam.

It seems interesting to compare the EC buildup in the MI with other storage rings. The sudden onset of a significant EC signal as a function of N_b, and the actual value of $N_{b,th}$, are related to a combination of vacuum chamber parameters (both physical and electronic), bunch length and bunch spacing. Simulations for the EC buildup in the LHC arc dipole magnets, for example, show a gradual (essentially linear) dependence of the EC power deposition as a function of $(N_b - N_{b,th})$, where $N_{b,th} \sim 2 \times 10^{10}$ [19, 20]. This behavior appears to be qualitatively different from the MI; it is likely that the much longer bunch spacing in the LHC plays an essential role in explaining the difference. More research is needed to clarify these

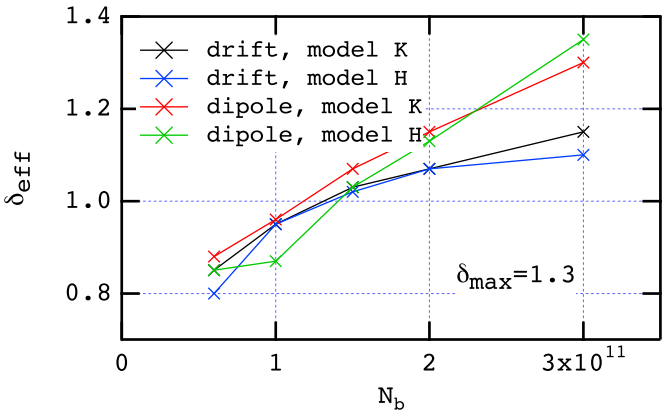

FIG. 6: The effective SEY, $\delta_{\rm eff}$, vs. bunch intensity N_b. The threshold $N_{b,th} \simeq 1.25 \times 10^{11}$ is the value of N_b at which $\delta_{\rm eff}$ crosses 1, consistent with the results in Fig. 4.

issues.

As mentioned in Sec. II B, the choice $\delta_{\rm max} = 1.3$ in this preliminary assessment is meant as a first step in a more complete analysis. We have chosen this value for $\delta_{\rm max}$ because it is believed to correspond to more or less well conditioned stainless steel. The EC effect is a self-conditioning phenomenon in the sense that the very same electrons from the cloud condition the vacuum chamber as they strike its surface during normal machine operation, leading to a gradual decrease of $\delta_{\rm max}$ and hence to a diminished EC effect [21, 22]. The electron dose required to reach an innocuous EC effect, is, roughly speaking, $\sim 0.1 - 1$ C/cm^2. For the MI conditions studied in this article, the average electron flux at the walls (see Fig. 3 caption) is $\sim 10^{-10}$ A/cm^2 for $N_b = 6 \times 10^{10}$, implying a self-conditioning time of hundreds of years. On the other hand, at $N_b = 3 \times 10^{11}$, the electron flux at the walls is 6 orders of magnitude larger, implying a self-conditioning time of hours. Of course, this analysis is very simplistic, as many other factors affect the conditioning time; nevertheless, the electron flux gives a rough estimate of the relevant time scales.

As seen in Table I, the backscattered component of the SEY at $E_0 = E_{\rm max}$ is $(\delta_e(E_{\rm max}) + \delta_r(E_{\rm max}))/\delta(E_{\rm max}) = 0.41$ for model K and 0.10 for model H. In the regime of interest to the MI this implies that, in SEY model K, the electrons are emitted with higher average energy than in model H. The higher energy implies a faster traversal across the chamber, and an effectively higher yield in subsequent electron-wall collisions, which helps to explain why ρ_e, $\delta_{\rm eff}$ and $1/\tau$ are higher in the former model than in the latter (see Figs. 4, 5 and 6 for a more complete set of results).

A set of delicate measurements of $\delta(E_0)$ and $d\delta/dE$ for copper samples at low temperature ($T \simeq 9$ K) carried out by Cimino and Collins at CERN [23] exhibits an upturn in $\delta(E_0)$ as E_0 decreases below $\sim$ 20 eV, reaching $\delta(0) \simeq 1$ (an indication of a similar upturn is apparent in another set of measurements: see Ref. 24, Fig. 5). The Cimino-Collins data exhibit the usual conditioning effect whereby $\delta_{\rm max}$ gradually decreases with electron bombardment. However, the data also exhibit the novel feature that $\delta(E_0)$ is insensitive to electron bombardment for $E_0 \lesssim 10-20$ eV. Measurements of the spectrum $d\delta/dE$ for several values of E_0 allowed the extraction of $\delta_e(E_0)$ and $\delta_r(E_0) + \delta_{ts}(E_0)$, which showed that $\delta_e(E_0) \to 1$ in the limit $E_0 \to 0$ regardless of the state of conditioning of the sample, while $\delta_r(E_0) + \delta_{ts}(E_0) \to 0$ in the same limit. Since $\delta_{ts}(E_0) \to 0$ in this limit, these measurements imply $\delta_r(0) = 0$. By contrast, in the models used here for the MI simulations, $\delta(E_0)$ decreases monotonically as $E_0 \to 0$, and its three components have the following values: model K: $\delta_e(0) = 0.32$, $\delta_r(0) = \delta_{ts}(0) = 0$; model H: $\delta_e(0) = 0.31$, $\delta_r(0) = 0.07$, $\delta_{ts}(0) = 0$. EC buildup simulations showed that the upturn in the Cimino-Collins data leads to a substantially larger EC signal relative to the more conventional model in which $\delta(E_0)$ decreases monotonically as $E_0 \to 0$ [25]. This relatively large effect of the low-energy details of the SEY can very likely be attributed to the long survival time in the vacuum chamber of the backscattered electrons when the bunch spacing is sufficiently large, as in the LHC [19]. For the case of the MI, the much shorter bunch spacing diminishes the relative importance of the backscattered electrons. A simulation spot check of the EC buildup for $N_b = 3 \times 10^{11}$ (results not shown) with a SEY model corresponding to the Cimino-Collins data showed that the exponential growth time τ is somewhat larger than the results in Sec. III B, although in general there were no qualitative differences.

The essential parameters that determine $N_{b,th}$ are almost certainly $\delta_{\rm max}$, $E_{\rm max}$ and $\delta(0)$. It seems imperative, therefore, to determine $N_{b,th}$ as a function of these three quantities. In addition, the beam energy may play an important, but indirect, role primarily through the bunch length σ_z. At top energy, $E_b = 120$ GeV, σ_z is shorter by a factor of 5 relative to injection energy. This shorter bunch length probably leads to longer high-energy tails in the E_0 spectrum, and therefore to a possibly higher value of $\delta_{\rm eff}$ relative to the injection-energy case. The dependence of $N_{b,th}$ on σ_z should, therefore, also be established. However, once threshold is exceeded, the saturated value of the EC density is probably always comparable to the beam neutralization level, which is independent of beam energy. Therefore, above threshold, the tune shift follows the rather simple scaling $\Delta\nu \sim 1/E_b$, which leads to the estimate $\Delta\nu \simeq 3 \times 10^{-3}$ at $E_b = 120$ GeV.

For simplicity, we have assumed a tri-gaussian density distribution for the bunch, with round aspect ratio in the transverse plane. In reality, the bunch has an elliptical aspect ratio owing to the variation of the β function, while the longitudinal profile is probably not quite gaussian. The dependence of our results on deviations from these simplifying approximations should be quantified, and an assessment of the EC density in other magnets,

especially quadrupoles, should be investigated.

In addition to the above-mentioned possible dependencies on physical parameters, the simulation parameters should also be checked for numerical stability. In the cases presented here, we have taken bunch length effects into consideration by dividing the full bunch length into 10 equal time steps, (ie., $N_k = 11$ kicks), and the inter-bunch spacing into $N_g = 9$ steps. Given the beam parameters, this slicing leads to time steps of size $\Delta t \simeq 1$ ns both within the bunch and in between bunches. The EC space-charge forces are computed and applied at every time step by means of a 2D grid of size 5 mm$\times$5 mm. The N_e primary electrons, Eq. (5), are represented by $M_e = 10$ macroparticles of charge $Q/e = N_e/M_e = 411.6$. The rather low value of M_e accounts for the noisiness of the EC line density for $N_b = 6 \times 10^{10}$, Fig. 2a, but it is practically inconsequential above threshold. From our experience with EC simulations for other storage rings, it appears that these simulation parameters provide approximately stable results, although methodical tests remain to be carried out.

Acknowledgments

I am grateful to A. Chen, W. Chou, K. Y. Ng, J.-F. Ostiguy, P. Yoon and X. Zhang for valuable discussions.

[1] Proton Driver Study. II. (Part 1, ch. 13), FERMILAB-TM-2169 (G. W. Foster, W. Chou and E. Malamud, eds.), May 2002.

[2] Proc. *Mini-Workshop on Electron-Cloud Simulations for Proton and Positron Beams "ECLOUD'02"* (CERN, April 15-18, 2002; F. Zimmermann and G. Rumolo, eds.), CERN Yellow Report CERN-2002-001 (2002), http://slap.cern.ch/collective/ecloud02/

[3] Proc. *31st ICFA Advanced Beam Dynamics Workshop on Electron-Cloud Effects "ECLOUD'04"* (Napa, April 19-23, 2004; M. Furman, S. Henderson and F. Zimmermann, eds.), CERN Yellow Report CERN-2005-001/CARE-Conf-05-001-HHH/LBNL-56372/SNS-10400000-TR0024-R00, http://icfa-ecloud04.web.cern.ch/icfa-ecloud04/

[4] Proc. *33rd ICFA Advanced Beam Dynamics Workshop on High Intensity and High Brightness Hadron Beams "ICFA-HB2004"* (Bensheim, October 18-22, 2004; I. Hofmann and J.-M. Lagniel, eds.), AIP Conference Proceedings **773**, BNL-73262-2004-AB (2004), http://www.gsi.de/search/events/conferences/ICFA-HB2004/index_e.html

[5] ICFA Beam Dynamics Newsletter No. 33 (K. Ohmi and M. Furman, eds.), http://www-bd.fnal.gov/icfabd/news.html.

[6] M. A. Furman and G. R. Lambertson, "The electron-cloud instability in the arcs of the PEP-II positron ring," LBNL-41123/CBP Note-246, PEP-II AP Note AP 97.27 (Nov. 25, 1997). Proc. *Intl. Workshop on Multibunch Instabilities in Future Electron and Positron Accelerators "MBI-97"* (KEK, 15-18 July 1997; Y. H. Chin, ed.), KEK Proceedings **97-17**, Dec. 1997, p. 170.

[7] M. A. Furman, "The electron-cloud effect in the arcs of the LHC," LBNL-41482/CBP Note 247/LHC Project Report 180 (May 20, 1998).

[8] M. A. Furman and M. T. F. Pivi, "Probabilistic model for the simulation of secondary electron emission," LBNL-49771/CBP Note-415 (Nov. 6, 2002). PRST-AB **5** 124404 (2003), http://prst-ab.aps.org/pdf/PRSTAB/v5/i12/e124404.

[9] M. A. Furman and M. T. F. Pivi, "Simulation of secondary electron emission based on a phenomenological probabilistic model," LBNL-52807/SLAC-PUB-9912 (June 2, 2003).

[10] M. Reiser, *Theory and Design of Charged Particle Beams*, J. Wiley & Sons, 1994, Sec. 4.6.

[11] R. Macek, private communication.

[12] M. A. Furman, "Formation and dissipation of the electron cloud," LBNL-51829, Proc. PAC03 (Portland, May 12-16, 2003), paper TOPC001.

[13] V. Baglin, J. Bojko, O. Gröbner, B. Henrist, N. Hilleret, C. Scheuerlein, M. Taborelli, "The secondary electron yield of technical materials and its variation with surface treatments," LHC-PR-433, 23 Sept. 2000. Proc. EPAC00, paper THXF102

[14] V. Baglin, I. Collins, O. Gröbner, B. Henrist, N. Hilleret, G. Vorlaufer, "Secondary electron emission: experimental results and their implications," Proc. *Intl. Workshop on Two-Stream Instabilities in Particle Accelerators and Storage Rings* (KEK, Sept. 11-14, 2001), http://conference.kek.jp/two-stream/ (talk given by N. Hilleret).

[15] V. Baglin, I. Collins, B. Henrist, N. Hilleret, G. Vorlaufer, "A summary of main experimental results concerning the secondary electron emission of copper," LHC Project Report-472 (2 Aug. 2001).

[16] R. E. Kirby and F. K. King, "Secondary Electron Emission Yields From PEP-II Accelerator Materials," SLAC-PUB-8212 (Oct. 2000). NIMPR A **469**, 1-12 (2001).

[17] M. A. Furman, "Effective theory of the electron cloud formation and dissipation," in progress.

[18] M. A. Furman and A. Zholents, "Incoherent effects driven by the electron cloud," LBNL-42688/CBP Note 286 (Mar. 29, 1999). Proc. PAC99 (New York City, March 29-April 2, 1999), p. 1794 (paper TUP130).

[19] M. A. Furman and V. H. Chaplin, "Update on electron-cloud power deposition for the Large Hadron Collider arc dipoles," LBNL-59062/CBP Note 723 (January 30, 2006). PRST-AB **9** 034403 (2006), http://prst-ab.aps.org/pdf/PRSTAB/v9/i3/e034403

[20] D. Schulte and F. Zimmermann, "Electron cloud build-up simulations using ECLOUD," Proc. ECLOUD'04 [3], p. 143

[21] J. M. Jiménez, G. Arduini, P. Collier, G. Ferioli, B. Henrist, N. Hilleret, L. Jensen, L. Weiss and F. Zimmermann, "Electron cloud with LHC-type beams in the SPS: a review of three years of measurements," LHC Project Report 632 (8 Apr. 2003). Presented at the *Mini-Workshop*

on SPS Scrubbing Run Results and Implications for the LHC (CERN, 28 June 2002).

[22] R. J. Macek, A. A. Browman, M. J. Borden, D. H. Fitzgerald, R. C. McCrady, T. Spickermann and T. J. Zaugg, "Status of experimental studies of electron cloud effects at the Los Alamos Proton Storage Ring," Proc. ECLOUD'04 [3], p. 93.

[23] R. Cimino and I. R. Collins, "Vacuum chamber surface electronic properties influencing electron cloud phenomena," LHC Project Report 669 (25 Aug. 2003). Proc. *8th European Vacuum Conference and 2nd Annual Conference of the German Vacuum Society* (Berlin, 23–26 June 2003; J.-J. Pireaux, R. Wiesendanger and K. Jousten, eds.). Applied Surface Science **235**(1), pp. 231–235, July 2004.

[24] B. Henrist, N. Hilleret, M. Jiménez, C. Scheuerlein, M. Taborelli, G. Vorlaufer, "Secondary electron emission data for the simulation of electron cloud," Proc. ECLOUD'02 [2], p. 75.

[25] R. Cimino, I. R. Collins, M. A. Furman, M. Pivi, F. Ruggiero, G. Rumolo, and F. Zimmermann, "Can low energy electrons affect high energy physics accelerators?," CERN-AB-2004-012 (ABP)/LBNL-54594/SLAC-PUB-10350 (Feb. 9, 2004). Phys. Rev. Lett. **93**, 014801 (2004).

DISCLAIMER